J. Fluid Mech. (1974), *vol.* 65, *part* 4, *pp.* 735–751
Printed in Great Britain

Experimental and theoretical studies of dissolution roughness

By PAUL N. BLUMBERG† AND RANE L. CURL
Department of Chemical Engineering, University of Michigan, Ann Arbor

(Received 2 August 1973 and in revised form 9 April 1974)

Periodic dissolution patterns that result from the interaction of a soluble surface and an adjacent turbulent flow have been investigated experimentally and theoretically. They occur at a Reynolds number based on a characteristic wavelength and friction velocity of about 2200. Experimental results for the stable geometry, propagation, mass-transfer distribution, average mass-transfer correlation and friction factor are presented. An interpretation based upon the repetitive transitional nature of the flow structure is advanced to explain aspects of the origin and behaviour of this type of roughness.

1. Introduction

In convective transport the flow field and diffusive properties establish the distribution of the rate of heat or mass transfer from a surface. If the surface is soluble, an interaction between the flow and any surface irregularity can lead to the development of a rough surface with the surface shape responding to the local distribution of dissolution and this, in turn, creating new boundary conditions for the adjacent flow. The complexity of these 'bed forms' has been documented by Allen (1971*a*, *b*), especially for their transient development from initial surface defects. The final, quasi-steady surface roughness configuration has been given the name *scallops* in the geological and speleological literature. An apparently special form of scalloping produces ripple-like forms with subparallel crests normal to the direction of flow, which have commonly been given the name *flutes* (Allen used the term 'flute' for certain transient forms). Both of these forms are illustrated in figures 1(*a*) and (*b*) (plate 1), from limestone and ice caves. Descriptions, discussions and bibliographies on the natural occurrence of these and related flow-created roughness forms can be found in Allen (1971*a*, *b*), Goodchild & Ford (1971) and Curl (1966).

If a surface irregularity is sufficiently pronounced, the adjacent flow will separate and reattach downstream from the disturbance. A mass-transfer-rate distribution will result with high rates in the vicinity of the point of reattachment and lower rates in the region of separation and recirculation. With continued dissolution a concavity or trough tends to form and spread downstream. If flutes develop, an equilibrium pattern (figure 2) may result and be stable in the sense that the local mass-transfer-rate distributions remain consistent with the

† Present address: Ford Motor Company, Dearborn, Michigan.

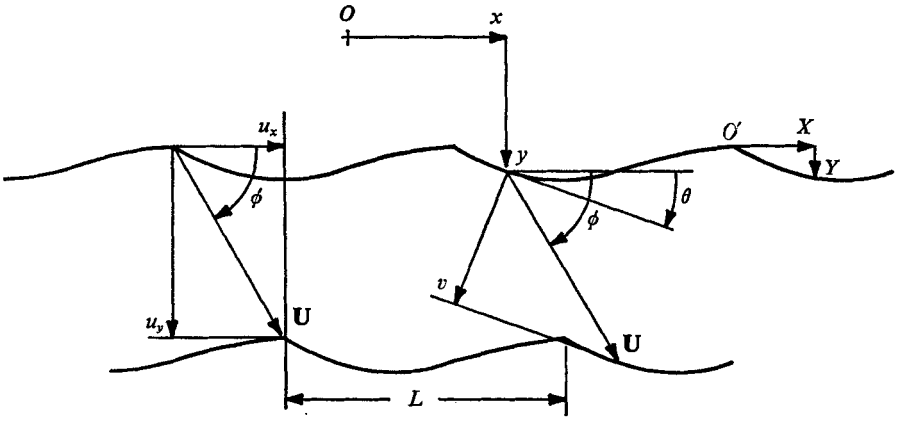

FIGURE 2. Flute geometry and propagation. Dissolution-rate and propagation vectors are shown to scale. The lower profile shows location after dissolution at a propagation angle $\phi = 61°$.

geometry. The surface then dissolves with no further change in shape. An equilibrium scalloped surface is probably only stable in a statistical sense.

A remarkable property of fluted and scalloped surfaces is the apparent dependence of the length scale L on the ratio U/ν of the velocity to the kinematic viscosity. In observing active limestone–water and ice–air flute systems, Curl (1966) noted that the Reynolds numbers based on the wavelength and mainstream velocity for the two cases were roughly 23000, despite an order-of-magnitude difference in kinematic viscosity. This was found consistent with simple dimensional considerations, leading to the prediction of a constant-period Reynolds number for flutes.

Although the phenomenon of flutes bears some resemblance to other periodic phenomena, such as the formation of sediment ripples and wave generation by wind action, it has two distinguishing features. First, the solid material dissolves and is removed and is not redeposited. Second, the phenomenon produces a roughness form on which flow separation occurs at each crest. Theoretical studies of transport with flow over wavy surfaces (Benjamin 1959) and experimental studies of evolving wavy surfaces (Ashton & Kennedy 1972) and sediment transport processes (e.g. Kennedy 1964; Allen 1968) are not directly relevant here, although the first two would be relevant to certain aspects of the initiation of dissolution roughness.

Although dissolution roughness involves mass transfer it is basically a hydrodynamic phenomenon in which the flow boundary condition is evolutionary. It should be possible from a study of both the flow and the surface to deduce the hydrodynamic factors involved in the origin, scale determination and propagation of dissolution roughness. We shall present here geometric and dimensional relationships pertaining to the properties primarily of equilibrium flutes, and results of laboratory experiments in which these properties, including mass and momentum transfer, have been measured. Finally, we present proposals based on observations for the hydrodynamic origin of the characteristic dimensional scaling of dissolution roughness with solvent velocity.

2. Geometric relations

The geometric and propagation properties of dissolution roughness reveal certain aspects of the adjacent flow or, more precisely, the effect of the adjacent flow on the local rate of dissolution. Consider a co-ordinate system fixed with respect to the solid soluble surface with the co-ordinate x parallel to the mean surface and y normal to and into this mean surface (figure 2, origin O). The slope angle θ at a point (x, y) on the surface and y are both functions of x and the time t. The dissolution-rate velocity v, normal to the surface, is in general also a function of x and t. If the surface were multi-valued (in y), v would be also, but this situation will not be considered further. The general surface-shape evolution relation is given by

$$\partial y/\partial t = v \sec\theta. \tag{2.1}$$

The general transient evolution of a soluble rough surface is a difficult problem but, because v is at present an unknown function of a general turbulent flow, primarily the equilibrium form of roughness will interest us here. Such a pattern will propagate in the x direction at some velocity u_x and the y direction at u_y, both of which may be functions of time. The resultant propagation velocity $\mathbf{U} = (u_x, u_y)$ makes an angle ϕ with the x axis. The general condition for the preservation of the equilibrium form is

$$y - \int_0^t u_y\,dt = f\left(x - \int_0^t u_x\,dt\right), \tag{2.2}$$

which gives, with (2.1),

$$u_y - u_x f' = v \sec\theta. \tag{2.3}$$

Normalizing with respect to the average dissolution rate u_y, and after some rearranging, we obtain

$$v/u_y = \sin(\phi - \theta)/\sin\phi. \tag{2.4}$$

If the surface solute concentration is constant, this is also the ratio $h/\bar{h}$ of the local to the average mass-transfer coefficient. Although θ can be obtained from a flute profile, it is not sufficient to determine ϕ, and hence the dissolution-rate pattern over the surface. The propagation angle can only be determined experimentally.

The idealized flute form is a periodic pattern with crests and troughs. A co-ordinate system may be defined with respect to the crests as shown in figure 2, when the surface shape is given by $Y(X)$. For the equilibrium pattern this transformation is trivial and does not alter the relation for the dissolution-rate pattern given by (2.4), which depends only upon surface and propagation angles.

The crests of natural flutes are observed to be not absolutely sharp, which may be because the soluble material is not absolutely homogeneous, or because of the nature of the process itself. Because natural crests are observed to be nearly sharp, and because the crest is a useful origin for measuring flute geometry, it is worthwhile to investigate crest propagation itself. It may be shown from (2.1) that a profile point where the slope is θ appears to propagate at the angle ϕ' given by

$$\tan\phi' = \tan\theta - \frac{\sec^3\theta}{r\,\partial[\ln(v\sec\theta)]/\partial x}, \tag{2.5}$$

where r is the radius of curvature of the surface at that point. At the top of a crest (or at the bottom of a trough), where θ is zero, this becomes

$$r = -\frac{\cot\phi'}{\partial \ln v/\partial x}. \tag{2.6}$$

The radius of curvature of an equilibrium crest is therefore inversely proportional to the local rate of change of the logarithm of the dissolution rate.

Compared with the flute period or other dimensions, r at a crest is actually very small. Equation (2.5) becomes indeterminate in the limit $r \to 0$ and a different calculation is needed to determine the propagation angle from crest dissolution processes. If (2.4) is applied to any two points in an equilibrium pattern, u_y may be eliminated to give

$$\tan\phi = \frac{v_1 \sin\theta_2 - v_2 \sin\theta_1}{v_1 \cos\theta_2 - v_2 \cos\theta_1}. \tag{2.7}$$

The points, numbered 1 and 2, may then be chosen to be the lee and streamward sides of an abrupt crest (a 'corner' with $r = 0$), giving the propagation direction in terms of local conditions. This would also apply to non-equilibrium crests. For all practical purposes (2.7) is applicable to the real situation.

3. 'Universal' laws of dissolution roughness

A simple dimensional analysis to show that the flute period, or some characteristic dimensions of scallops, should scale such that a Reynolds number based on that dimension remains constant has been proposed (Curl 1966). The mean channel velocity was used. Blumberg (1970) adopted the maximum velocity U_m in the vicinity of the wall while Goodchild & Ford (1971) used the velocity 3 cm above the surface.

It has since become apparent that the velocity conditions near the wall depend upon the channel size, given either the mean or maximum channel velocity. The conclusion is that a 'law of the wall' turbulent-flow analysis is a better basis for a dimensional analysis of flute or scallop geometric properties. If it is assumed that a rough fluted or scalloped surface is given *a priori*, and is described by a set $\mathscr{L}$ of either fixed geometric properties (dimensions) for flutes or statistical geometric properties for scallops, the average-velocity profile u of the fluid near the wall depends upon the average wall shear stress τ, a characteristic dimension L of the pattern, the distance y from the surface, the normalized roughness geometry $\mathscr{L}/L$, the fluid density ρ and the kinematic viscosity ν. Experiments have shown that this may be represented approximately by the well-known universal velocity distribution law

$$u/v^* = 2{\cdot}5 \ln y/L + B_L, \tag{3.1}$$

where v^* is the friction velocity $(\tau/\rho)^{\frac{1}{2}}$. The roughness function B_L must depend on the geometry $\mathscr{L}/L$ and the roughness friction Reynolds number $Re^* = Lv^*/\nu$. Schlichting (1937) explored a wide variety of patterned roughness forms and found this relation to apply. Because flutes or scallops are no more exotic than

the roughness elements used by Schlichting, we shall presume that (3.1) applies also in the present situation.

The above discussion avoids the central issue that the dissolution of a soluble wall creates the roughness form which in turn determines the near-wall turbulence structure. To examine this question imagine a turbulent flow over a soluble surface where the average wall shear stress is fixed. Some dissolution pattern will evolve and, when equilibrium is reached, it may be presumed that any characteristic dimension L of the pattern will depend on the shear stress, fluid properties and possibly the molecular diffusivity D of the solute. From dimensional arguments one obtains

$$Re^* = Lv^*/\nu = f(\nu/D). \tag{3.2}$$

Given the Schmidt number $Sc = \nu/D$, the equilibrium value of Re^* must be a constant. It also follows, by extending (3.2) to any length dimension, that all flute (or scallop) patterns should have a universal geometry (i.e. $\mathscr{L}/L$ is a universal set), possibly dependent on Sc. Returning now to (3.1), we see that B_L must also be a constant for equilibrium flutes (scallops) and is equal to the ratio $u(L)/v^*$.

The average surface shear stress ρv^{*2}, expressed in the form $\frac{1}{2}\rho u^2(L) f_L$, gives a wall friction factor $f_L = 2B_L^{-2}$. It is convenient to use $u(L) = v^* B_L$ as a characteristic near-wall velocity, rather than the mean or maximum channel velocity, or even the friction velocity v^*, because it has a simple physical interpretation. If the velocity profile were moderately flat we would expect $u(L)\,L/\nu = Re_L$ to be close to the previously estimated value of 23 000. The evaluation of B_L and Re^* from measurements of velocity profiles over equilibrium flutes and scallops will be reported and discussed later.

Integration of (3.1) from the wall to the centre of a circular channel will relate the mean channel velocity $\bar{u}$ to the equilibrium flute size. The result,

$$\bar{u}L/\nu = Re^*\{2{\cdot}5[\ln(R/L) - \tfrac{3}{2}] + B_L\}, \tag{3.3}$$

is useful for estimating paleohydrologic conditions in natural fluted conduits (Curl 1974). The conduit Fanning friction factor $\bar{f} = 2\tau/\rho\bar{u}^2 = 2(v^*/\bar{u})^2$, in terms of the Reynolds number $\overline{Re}_d$ based on the conduit diameter and mean velocity, follows from (3.3):

$$\bar{f}^{-\frac{1}{2}} = 1{\cdot}77 \ln(\overline{Re}_d \bar{f}^{\frac{1}{2}}) - (4{\cdot}49 + 1{\cdot}77 \ln Re^* - 0{\cdot}707 B_L). \tag{3.4}$$

This is identical in form to Prandtl's universal resistance law for smooth pipes at large Reynolds numbers. That is, the conduit with dissolution roughness that is always adapted to the flow conditions acts as a *pseudo-smooth rough pipe*. This result could have been perceived sooner by noting that there does not actually exist any *a priori* roughness scale in the case of dissolution roughness and therefore (following Prandtl's smooth-pipe analysis) L in (3.1) could have been chosen from the first as proportional to ν/v^*.

From (3.2) we can also conclude that

$$\phi = f(Sc), \quad \hat{Y} = f(\hat{X}, Sc), \tag{3.5), (3.6}$$

where $\hat{Y} = X/L$ and $\hat{X} = X/L$ are dimensionless flute co-ordinates.

A dimensional analysis for the local mass-transfer coefficient, based on the friction velocity v^*, yields

$$hL/D = f(Re^*, \hat{X}, Sc). \tag{3.7}$$

The profile of the local mass-transfer rate must be *similar* at fixed Schmidt number. The degree to which it varies with the Schmidt number must be determined experimentally (as must also the Schmidt-number dependencies in (3.2), (3.5) and (3.6)). If, at equilibrium, Re^* is essentially independent of Sc, as will be argued later, and is therefore a constant, it need not be included in (3.7).

Averaging (3.7) over a single flute period shows that the average Nusselt number Nu^* depends only on the Schmidt number. It would be expected to be approximately proportional to $Sc^{\frac{1}{3}}$, by analogy with other boundary-layer-dominated transfer processes.

4. Apparatus and experimental measurements

The aims of the experiments were to generate stable flutes, to measure their geometric and propagation properties, to determine their transport properties and, if possible, to ascertain the hydrodynamic mechanisms responsible for their various characteristics. The equipment was designed to provide a sufficiently rapid flow at controlled velocities, temperatures and undersaturation over a soluble surface. Plaster of Paris (gypsum), suggested by Rudnicki (1960) and used also by Allen (1971*a*) and Goodchild & Ford (1971), was chosen as the substrate as it has a reasonable but low solubility and, more important, is easily cast to a suitable size and shape. A recirculating flow in a 6×6 in. water tunnel was driven by a propeller through a honeycomb flow straightener and over the plaster block. The block, 30 in. long, 6 in. wide and 5 in. deep, was cast as free of air bubbles as possible and its sides and ends were protected from dissolution with shellac. The block was supported on a plate which could be raised as dissolution proceeded.

The temperature was controlled automatically to within 1 °C and the concentration of calcium sulphate in solution was kept constant (at about 10 % of saturation) by a metered flow of fresh tap water accompanied by an equal overflow from the system. The pH of the system was held at 6·0 by continuous addition of acetic acid in order to prevent formation of $CaCO_3$. Further details of the design of the apparatus and its operation may be found in Blumberg (1970).

Both scalloped and fluted surfaces were generated. Because the latter did not appear spontaneously in the dissolution distance available, the original flat surfaces were inscribed with transverse grooves at chosen intervals, from which flute profiles developed with relatively little dissolution. This procedure effectively prevented a direct determination of the stable, equilibrium Reynolds number for flutes but did allow a study of the behaviour of near-equilibrium and non-equilibrium spacings.

From timed measurements of the trajectories of the flute crests with respect to the block, values of ϕ and u_y could be determined. Subsequent careful measurements of the surface profiles with an indicator gauge gave local values of the

surface slope, permitting the complete dissolution-rate profile over a flute period to be determined [using (2.4)] as well as the average dissolution rate, from which the Nusselt number Nu could be estimated. Velocity profiles were measured with a liquid-filled Pitot tube and from these the apparent mean surface shear stress could be estimated using the logarithmic velocity law [equation (3.1)]. The channel was too short for the full development of the velocity profile, which was a difficulty in using velocity profiles for the accurate determination of Re^*.

Qualitative flow visualization experiments were carried out using either fine polyvinyl chloride particles, which indicated the average overall flow pattern, or potassium permanganate crystals, which, collecting and dissolving in the flute troughs, coloured the recirculating flow in the lee of the crest and indicated the structure of the shear layer between the separated main flow and the recirculating flow. The conditions of all experiments are reported in table 1.

5. Flute profile stability

Although equilibrium flutes were not generated from a flat surface, an estimate was available for the approximate stable-flute Reynolds number (Curl 1966). The initial experiments were conducted to determine what happens with large departures from what was expected to be the approximate relation between the flute wavelength and the velocity near the wall. Because v^* could not itself be chosen in advance (and also because previous analyses of flute stability had not yet brought in the concept of a wall friction Reynolds number as the 'universal' constant) the maximum mainstream velocity was chosen, in combination with the induced flute wavelength, to give a maximum-velocity Reynolds number Re_m near the previously suggested value of 22500. Two blocks were inscribed with transverse grooves at 2 in. intervals, from which flutes developed on dissolution. One block was used in an experiment (experiment 2) in which the 2 in. flutes were expected to be stable ($U_m = 42{\cdot}9$ cm/s, $Re_m = 23300$), and the other block at a higher velocity ($U_m = 80{\cdot}3$ cm/s, $Re_m = 25500$) at which the 1 in. flutes were expected to be stable (experiment 3). The results are shown in the photographs in figures 3 and 4 (plate 2).

In experiment 2 (figure 3) the 2 in. flute region was 'stable' for a vertical dissolution distance of over 2 in. On the other hand the 1 in. (at $Re_m = 11500$) flutes became obscure as dissolution proceeded. The effect near the end of the 2 in. flute region was, in fact, to suppress the height of alternate flute crests. The 1 in. flute instability was such as to increase the average wavelength of the pattern in this region. The irregular patterns developing near the edges of the blocks were due to side-wall boundary layers and are not related to stability or instability of the flute pattern itself.

In experiment 3 (figure 4, plate 2) a very different outcome was observed. Whereas the 1 in. flutes appeared moderately stable, small disturbances in the surface appeared at various places, but especially on the streamward (stoss) slopes, within the group of induced 2 in. flutes. The apparent Re_m in this region was 51000. This type of instability is quite different from that observed in experiment 2. Its effect is to decrease the average wavelength of the pattern

Experiment	T (°C)	U_m (cm/s)	L (cm)	X (cm)	B_L	$Re^* \times 10^{-3}$	$Re_L \times 10^{-3}$	ϕ	$Nu \times 10^{-3}$	Sc	f_L
1.1	15·8	45·0	6·0†	—	§ —	—	—	—	1·53	1565	—
2.1	23·0	42·9	5·08	12·7	7·2	3·56	25·6	62°	1·10	1080	0·039
2.2	23·0	42·9	5·08	48·3	7·9	3·08	24·3	—	—	—	0·032
3.1	30·0	80·3	2·54	49·5	8·4	2·53	21·1	60°	0·97	788	0·028
3.2	30·0	80·3	2·54	57·1	11·2	1·92	21·6	75°‡	—	—	0·016
4.2	32·5	115·6	1·72†	53·4	8·8	2·32	20·5	—	1·18	710	0·026
4.3	32·5	115·6	1·72	53·4	9·9	2·12	21·0	—	—	—	—
6.1	27·6	113·0	1·91	19·1	9·6	2·33	22·4	59°	1·14	875	0·022
6.2	27·6	113·0	1·91	53·4	11·7	1·92	22·5	—	—	—	0·015
6.3	27·6	113·0	1·91	53·4	10·3	2·12	21·8	—	—	—	0·019
6.4	27·6	113·0	1·91	19·1	8·5	2·66	22·7	—	—	—	0·028
7.2	44·5	83·8	1·91	16·5	9·0	2·71	24·4	64°	0·89	443	0·025

† $\bar{L}_{32}$. ‡ Unstable 2 in. flutes. § Not measured.

TABLE 1. Experimental conditions and results. X is the distance from the leading edge of the block at which the velocity profile was measured

through initially small features increasing in size and number and 'consuming' the original pattern. We can conclude that, at least at the extreme 'near wall' values of Re_m of 11 650 and 51 000, flute patterns disintegrate rapidly in such a way as to tend towards an Re_m between these limits. How close the chosen 'stable' values of Re_m may be to the 'true' value is not disclosed by these two experiments.

In experiments 6 and 7 (not shown), 0·75 in. induced flutes were produced at 27·6 °C and 44·5 °C respectively, with the velocities (see table 1) adjusted to give essentially the same Re_m (25 600 and 26 000 respectively), but Schmidt numbers differing by a factor of two. In both cases the patterns were stable for dissolution distances exceeding two wavelengths. The Schmidt number does not have a dominant influence on flute-pattern stability.

Two experiments were made starting with a flat surface without inducing flutes (experiment 1) and with a randomly roughened surface (experiment 4), respectively. Both evolved into scalloped surfaces as shown in figure 5 (plate 3). By running the experiments at 15·8 and 32·5 °C and velocities of $U_m = 45{\cdot}0$ and 115·6 cm/s, respectively, values of U_m/ν differing by a factor of nearly four were established. The dissolution process responded as shown in the figure. The maximum longitudinal length of each 'scallop' concavity was measured and a mean size, $\bar{L}_{32}$ was calculated as the sum of cubes divided by the sum of squares. This mean value suppresses the importance of small concavities, which are questionable 'scallops', and brings the mean scallop dimensions into closer agreement with the friction measurements for flutes (§ 6). The observed values were $\bar{L}_{32} = 6{\cdot}0$ cm for experiment 1 and 1·72 cm for experiment 4. Converting to Reynolds numbers, the values of Re_m using these lengths were then 24 300 and 26 200, respectively. This is striking evidence of the Reynolds number domination of the length scale of a scalloped surface and the relative insensitivity to the Schmidt number.

The velocity U_m in terms of which the qualitative discussion of this section has been conducted is not the v^* or $u(L)$ that we expect to be most important in determining flute or scallop dimensions. However, it is appropriate for considering the qualitative observations of stability and instability, and the development of average scalloping dimensions.

6. Momentum transfer

Velocity profiles were measured over the sections of nominally stable flutes and over one scalloped surface. Because the channel was short the two boundary layers from the upper (smooth) and lower (fluted) surfaces were always developing and interacting. Nevertheless estimates of the friction velocity v^* were obtained by performing a regression analysis of the observations using (3.1). The results are given in table 1 as Re^*, B_L and f_L, and the first two are plotted in figure 6. 90 % confidence intervals for the measured v^* were used to construct the intervals shown in the figure. For comparison, a 90 % confidence region is shown for experiment 7.2. Because all of the velocity profile data were obtained over nominally stable dissolution patterns, and because the confidence intervals exhibit a strong correlation between Re^* and B_L estimates, it is not possible to

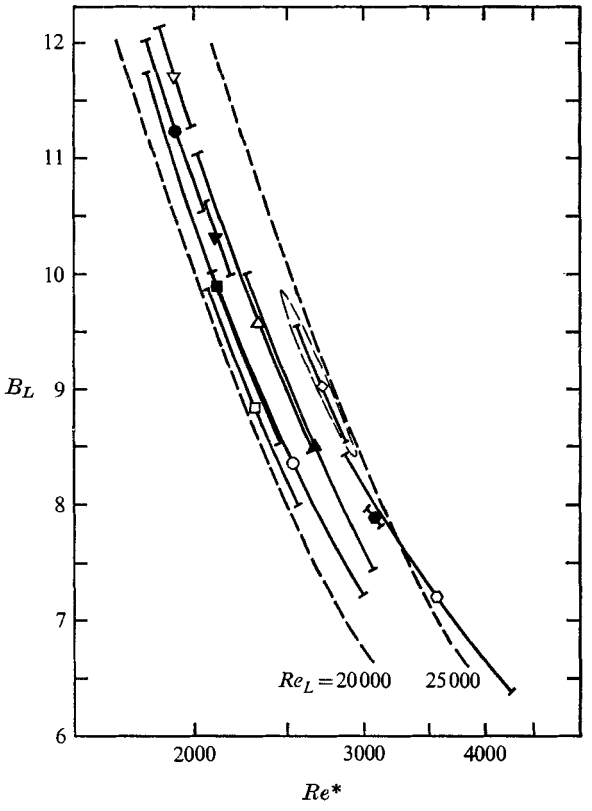

FIGURE 6. The dependence of the measured roughness function B_L on the friction-velocity Reynolds number Re^*. 90 % confidence intervals and lines (dashed) of constant

$$Re_L = B_L Re^*$$

are shown. Experiment numbers: ○, 2.1; ●, 2.2; ○, 3.1; ●, 3.2; □, 4.2; ■, 4.3; △, 6.1; ▽, 6.2; ▼, 6.3; ▲, 6.4; ◇, 7.1.

discern a phenomenological relation between them. For this purpose, experiments with fully developed channel flow would be needed.

Scallops are represented by the data from experiments 4.2 and 4.3, which are seen to fall among the values obtained from induced flutes (when $\bar{L}_{32}$ is used as the mean scallop dimension). To the extent, then, that $\bar{L}_{32}$ for scallops is equivalent to the wavelength of equilibrium flutes, the equilibrium values are $Re^* \doteq 2200, B_L \doteq 9.4$ and $Re_L \doteq 21\,000$. The flute friction factor is then $f_L \doteq 0{\cdot}023$. A much longer channel would be needed to improve on these values.

Schlichting (1937) made velocity profile measurements over 'long-angle roughness' bearing some resemblance to a fluted surface. For a wavelength/height ratio of 6·7 (compared with 8·0 for flutes) the values of B_L calculated from the results reported by Schlichting were constant at 7·1, but this was at values of Re^* from 7000 to 17 000. Schlichting's somewhat equivalent experiments were in the 'fully rough' regime and did not cover the transition-turbulence region where it appears that naturally evolving fluted and scalloped surfaces occur.

The value of $B_L = 7{\cdot}1$ is not an unreasonable lower limit in figure 6 for large values of Re^*, although this was not determined experimentally. The studies of Motzfeld (1937) on wavy walls were also made at large values of Re^*, exceeding about 10000.

With the above constants, equation (3.4) for the *pseudo-smooth rough pipe* becomes

$$\bar{f}^{-\frac{1}{2}} = 1{\cdot}77 \ln (\overline{Re_d} \bar{f}^{\frac{1}{2}}) - 11{\cdot}44. \tag{6.1}$$

The final constant would be $-0{\cdot}60$ for the smooth pipe (after Prandtl; see Schlichting 1968).

7. Flute geometry and propagation

Induced flutes were observed to adopt their final geometry, propagation direction and velocity within a short time after the initiation of dissolution. Figure 7 (plate 4) shows a typical flute profile from experiment 2. A number of measurements of flute profiles from a given experiment, and of flute profiles from different experiments, including flutes under unstable conditions (such as 2 in. flutes in experiment 3), suggested that neither the Reynolds number (stable or unstable) nor Schmidt number has a great effect on the flute profile. The explanation for this must lie in the details of the complex separating–reattaching flow following a crest. To obtain a representation of a stable profile, data from measurements of three stable flutes from each of experiments 2, 3 and 6 were normalized, pooled and fitted by a Fourier sine series using sufficient terms that the variance reduction ratio was not significant at the 1 % level. The result was

$$\hat{Y} = 0{\cdot}112 \sin \pi \hat{X} + 0{\cdot}028 \sin 2\pi \hat{X} - 0{\cdot}004 \sin 3\pi \hat{X} \tag{7.1}$$

and is shown in figures 2 and 8. For comparison there is also shown in figure 8 a composite profile from experiment 3, for 'unstable' 2 in. profiles. The difference is no more than that found among stable profiles from a single experiment.

Table 1 shows the measured values of the propagation angle, including that for unstable 2 in. flutes. Stable profiles propagate with a downstream component, characteristically at an angle of about $\phi = 61°$. The unstable 2 in. flutes of experiment 3 propagated instead at an angle $\phi = 75°$, prior to the development of the new, smaller scale, features that would lead to a new overall scale. The unstable 1 in. flutes from experiment 2 broke up before ϕ could be measured. From the profile, equation (7.1), and the direction of propagation for stable flutes, the complete mass-transfer profile may be obtained and is shown in figure 8, along with the result of applying the same analysis to unstable 2 in. flutes from experiment 3. While the geometric profiles are essentially the same, the distribution of mass transfer has been considerably altered.

Equation (2.4) can be written as

$$h/\bar{h} = \cos \theta - \cot \phi \sin \theta, \tag{7.2}$$

where θ is a nearly fixed function of $\hat{X}$, if the shape of an induced flute does not respond to velocity changes. Non-equilibrium (unstable) flow conditions, which change primarily ϕ, appear to change the admixture of the relatively fixed

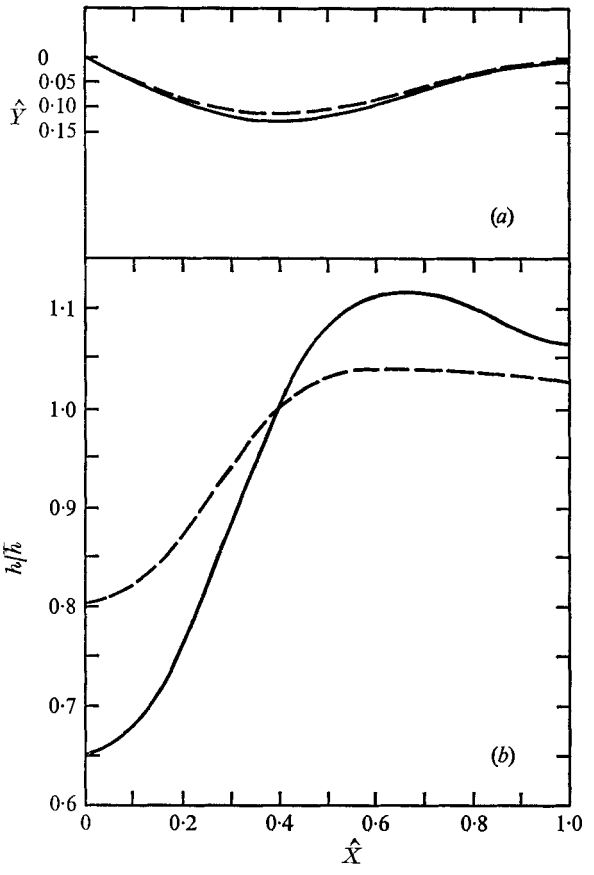

FIGURE 8. (*a*) Flute profile and (*b*) dissolution-rate profile. ——, 'stable' profiles, propagating at $\phi = 61°$; – – – –, 'unstable' profile, propagating at $\phi = 75°$ (from experiment 3).

functions $\cos\theta$ and $\sin\theta$ in the dissolution pattern. This is an interesting but unexplained flute property.

The crest in figure 8 (or figure 2) is shown as a sharp cusp. The radius of curvature of the crest was close to the granularity of the plaster, but it appeared to be of the order of 0·5% or less of the flute period. With $\phi = 61°$, equation (2.6) yields for the non-dimensionalized rate of change of the dissolution rate at the crest

$$\partial \ln v/\partial \hat{X} \doteq -110, \tag{7.3}$$

which shows the abrupt drop in dissolution rate at the flow separation point.

8. Mass-transport properties

The longitudinal variation of the average dissolution rate for both fluted and scalloped blocks was small and was not investigated. The average transfer coefficient for dissolution of both flutes and scallops, combined with the equilibrium flute or scallop dimension and a diffusivity ($D = 0{\cdot}90 \times 10^{-5}$ cm^2/s at

25 °C), gave the mass-transfer Nusselt numbers shown in table 1. A least-squares fit of Nu *vs.* Sc agreed with the conventional exponent of $\frac{1}{3}$. An adequate correlation for the *equilibrium* Nusselt number, from the results of the dissolution-rate experiments, is

$$Nu^* = 112\,Sc^{\frac{1}{3}} \tag{8.1}$$

for both flutes and scallops.

When applied to flow in an equilibrium scalloped or fluted conduit, the classical Colburn j factor for mass transfer becomes

$$j_m = \frac{\bar{h}}{\bar{u}} Sc^{\frac{2}{3}} = \frac{v^* Nu^* Sc^{-\frac{1}{3}}}{\bar{u}\, Re^*} = 0{\cdot}051 \left(\frac{\bar{f}}{2}\right)^{\frac{1}{2}}. \tag{8.2}$$

This is the same as the wall-region heat-transfer relationship for rough pipes that has been derived by Hughmark (1972). His constant, based upon mass-transfer data from smooth pipes, is 0.0816. The difference appears to be significant, but otherwise mass transfer on dissolution roughness behaves like that for other forms of roughness.

An estimate of the mass-transfer boundary-layer thickness $\delta_m = D/\bar{h}$ yields $\delta_m/L = Nu^{*-1} = 0{\cdot}0089\,Sc^{-\frac{1}{3}}$. For $Sc > 6$, δ_m is less than 0·5 % of L. This gives further reason to believe that the Schmidt number will have little effect upon the stability Reynolds number Re^*, flute profiles or propagation angle ϕ in aqueous solvents. Some effect may be expected in ice–air dissolution roughness.

9. Observations on flute hydrodynamics

The model shown in figure 9 illustrates the major observations of the hydrodynamics of stable dissolution profiles. Region 1 marks the inner edge of the main turbulent flow; the streamlines in this region are almost unaffected by the periodicity of the fluted surface. The position of flow separation is fixed by the sharpness of the flute crest. Coming into contact with the relatively slowly moving fluid in the lee cavity, the separated flow forms a 'laminar' free shear layer in region 2, which subsequently undergoes a transition to turbulence in region 3. The turbulence is responsible for the entrainment of fluid from the cavity and the consequent turning in of the flow towards the surface. Reattachment occurs in region 4, where part of the fluid moves downstream and part is returned into the cavity. The returned flow and free shear layer combined to provide a general recirculating motion in region 5. The flow is highly unsteady in the neighbourhood of reattachment (Curl 1966). Owing to a strong adverse pressure gradient, the returning boundary-layer flow formed along the lee slope separates before reaching the crest. This separation manifests itself in a small change in profile slope at the junction of regions 6 and 8. Region 8 consists of small eddies held between the shear layer and the separated recirculating flow. The boundary layer along the stoss slope separates from the downstream crest and, ideally, an identical flow pattern should be produced over the next flute.

The mass-transfer distribution on stable flutes (figure 8) exhibits a maximum at approximately $\hat{X} = 0{\cdot}62$. This may be considered as the average point of flow reattachment. As boundary layers develop from the reattachment point,

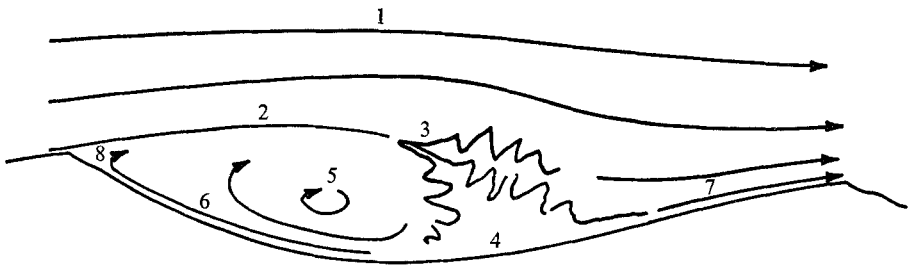

FIGURE 9. Hydrodynamic regions for flow over one flute period. (1) Main turbulent flow. (2) Laminar free shear layer. (3) Transition to turbulence and entrainment. (4) Reattachment. (5) Irregular recirculating flow. (6) Lee-slope boundary layer. (7) Streamward-slope boundary layer. (8) Lee-slope boundary-layer separation with small eddies.

the mass-transfer coefficient shows a continuous decrease in both directions. This maximum in the mass-transfer rate along the stoss slope is responsible for the downstream propagation angle of $\phi = 61°$.

In presenting the experimental mass-transfer distributions we have omitted the small effect of the lee-slope boundary-layer separation point. It is a feature of the profile, however, that is readily visible, occupying an interval of the normalized co-ordinate up to about $\hat{X} = 0{\cdot}05$.

The essential observed hydrodynamic feature of flow over dissolution profiles, stable or unstable, is the separation–transition–reattachment process. The distance between the upstream crest, i.e. separation, and the average point of flow reattachment determines that part of the surface which is exposed to maximum mass-transfer rates. If the Reynolds number is to influence the stable length scale, then the distance from separation to reattachment must be Reynolds-number dependent. The attachment to adjacent surfaces does not exhibit this dependence in completely turbulent separations. Turbulent jet experiments described by Sawyer (1962) and Newman (1961) showed that the position of reattachment was fixed by the geometry of the system alone. On the other hand, in studying transitional separations on airfoil sections, Gault (1955) showed that the distance from laminar separation to transition is dependent on the ratio U/ν and that, therefore, the reattachment of the separated flow is Reynolds-number dependent. In addition Chapman, Kuehn & Larson (1958) have observed that, in separating–reattaching flows, only those involving transition of the separated laminar flow display a Reynolds-number dependence. The value of the Reynolds number based on the length of the separated region is approximately 30000 in both of these studies. This is encouragingly close to $Re_L = 21\,000$.

The flow visualization experiments showed a relatively smooth, laminar separation and a downstream transition to turbulence in the shear layer. Dye experiments showed little or no turbulent mixing between the separated and recirculating flows immediately after separation (region 2), but intense mixing in the region of entrainment following transition. Residence times in the eddy region were at most a few seconds. Reasoning from stability observations, flow visualization experiments and the literature in related areas, we are led to the conclusion that shear-layer transition is a fundamental aspect of fully established flute hydrodynamics.

Stability

For the case in which the imposed Reynolds number is well below that required for flute stability, the point of shear-layer transition should move further out onto the stoss slopes, past $\hat{X} = 0{\cdot}62$. If this occurred on one profile, the boundary-layer thickness at the point of the next separation would be reduced, resulting in a more rapid development of an inflexion-point velocity profile in the shear layer, a more rapid transition and, consequently, a more rapid reattachment on the following profile. The higher residual turbulence in the shear layer would also tend to draw the position of reattachment closer to the subsequent crest. Of course, on a strictly periodic pattern, the flow must be strictly periodic (on the average) but, with any irregularities present, the flow might be expected to develop erratic patterns, sometimes reattaching 'short' and sometimes 'long'. This would destroy the original pattern (as observed) and lead to one of larger scale which would adapt better to the separating–transition–reattaching flow.

For the case in which the Reynolds number is well above that required for stability, a totally different type of instability was observed. This was characterized by the development of local 'pot holes' on the stoss slopes of the profiles, which then spread in the transverse direction. The rapid amplification of small disturbances on these portions of the profiles appears to be made possible by the flow structure which develops when the length scale is too long (or U/ν is too large). On a normalized basis, the transition of the shear layer to turbulence occurs closer to each crest. More fluid is entrained prior to reattachment, so that the effects of flow stagnation are felt over a larger portion of the stoss slope. This results directly in a flattening of the mass-transfer distribution along the streamward slope (figure 8), as compared with the decreasing coefficients observed in the stable case. When there is a flat mass-transfer distribution along the stoss slope a small disturbance leading to separation will produce a higher dissolution rate on the downstream side of the disturbance, thus amplifying it. In the stable case, on the other hand, the overall strongly decreasing transfer rate and the favourable pressure gradient just past reattachment probably combine to prevent renewed separation, or augmented dissolution if a small local separation does occur.

Scallop patterns, which we believe to have essentially the properties and origins described above for flutes, are much more common in nature. We do not know, however, whether or not there are any special conditions conducive to the origin of the two-dimensional flute forms. Constant temperature and flow velocity have been suggested as necessary conditions (Curl 1966) but the present work shows that these are not sufficient. It was thought that perhaps the solid side-wall boundaries prevented flute formation, but an experiment on a narrower block with open-ended induced flutes ended with the block scalloped. This question remains unanswered.

10. Comparison with other observations

The experiments of Goodchild & Ford (1971) suggest a value of 11500 for the equilibrium Reynolds number, based on a fluid velocity 3 cm from the surface and a number-mean scallop size. They also report observations of different average scallop sizes on adjacent limestone layers, in caves, which must have experienced the same flow velocity. The differences between their experiments and our results and this observation appear both to be related to imperfections (air bubbles in plaster or inclusions in limestone) that cause the initiation of small dissolution features that subsequently grow. The result is a smaller average scallop dimension.

The 'defect' origin of some scalloping patterns was a major theme of Allen (1971*b*). Allen found, however, that given sufficient dissolution distance on plaster of Paris, the mean scallop dimension tended to a limit. This gave $Re_L \doteq 17000$, based on the mean scallop length, but $Re_L \doteq 25000$, based on $\bar{L}_{32}$, which agrees closely with this work.

On the basis of the data of Carey (1966), who observed fluting on the underside of river ice, we obtain, assuming that (3.1) applies, Re_L ranging from 40000 to 80000. Ashton & Kennedy (1972) investigated both natural and artificial ripples formed during the freezing or melting of water ice. They found that, prior to the onset of flow separation at crests, the ripple period and mean flow velocity gave $Re_L \doteq 47000$. After separation occurred the period tended to decrease. Apparently, on ice, an initially dominant period can result from selective amplification of particular small amplitude surface-irregularity wavelengths. This does not appear to be an important mode in the generation of dissolution roughness on plaster of Paris. A possible explanation is that the heat conduction mechanism in freezing or melting tends to suppress small-scale irregularities resulting from local separation or reattachment.

None of the above workers reported velocity profiles from which Re^* could be determined.

An 'anomalous' wavy roughness in the Ecker Valley pipeline caused, ostensibly, by deposition of colloidal aluminium hydroxide, is discussed by Wiederhold (1949) and Seiferth & Kruger (1950). Applying (3.3) to their data, one finds $116 < Re^* < 662$, much smaller than in our system. It is possible that this phenomenon is related to separation–reattachment on the scale of the small lee crest feature that was observed for $0 < \hat{X} < 0{\cdot}05$.

The results in the above instances may also have involved processes other than just dissolution of a homogeneous solid. It also appears probable that there would be different regimes of interaction of flows and soluble surfaces, as there are for sand ripples and dunes. While the specific factors responsible for the differences described above are not entirely known, our results are supported by their internal consistencies over a wide range of conditions. More carefully controlled development of scallops (or possibly flutes) in a longer flume would be of value in identifying Re^* more precisely and possibly answering questions about the natural occurrence of flutes.

REFERENCES

ALLEN, J. R. L. 1968 On the criteria for the continuance of flute marks, and their implications. *Geol. en Mijnbouw*, **47**, 3.

ALLEN, J. R. L. 1971*a* Bed forms due to mass transfer in turbulent flows: a kaleidoscope of phenomena. *J. Fluid Mech.* **49**, 49–63.

ALLEN, J. R. L. 1971*b* Transverse erosional marks of mud and rock: their physical basis and geological significance. *Sedimentary Geol.* **5**, 167.

ASHTON, G. D. & KENNEDY, J. F. 1972 Ripples on underside of river ice covers. *Proc. A.S.C.E., J. Hydr. Div.* **98** (HY9), 1603.

BENJAMIN, T. B. 1959 Shearing flow over a wavy boundary. *J. Fluid Mech.* **6**, 161.

BLUMBERG, P. N. 1970 Flutes: a study of stable, periodic dissolution profiles resulting from the interaction of a soluble surface and an adjacent turbulent flow. Ph.D. dissertation, University of Michigan, Ann Arbor.

CAREY, K. L. 1966 Observed configuration and computed roughness of the underside of river ice, St. Croix River, Wisconsin. *U.S. Geol. Survey Prof. Paper*, 550-B, p. 192.

CHAPMAN, D. R., KUEHN, D. M. & LARSON, A. K. 1958 Investigation of separated flows in supersonic and subsonic streams with emphasis on the effect of transition. *N.A.C.A. Rep.* no. 1356.

CURL, R. L. 1966 Scallops and flutes. *Trans. Cave. Res. Group Brit.* **7**, 121.

CURL, R. L. 1974 Deducing flow velocity in cave conduits from scallops. *Bull. Nat. Speleo. Soc.* **36** (2), 1.

GAULT, D. E. 1955 An experimental investigation of regions of separated laminar flow. *N.A.C.A. Tech. Note*, no. 3505.

GOODCHILD, M. F. & FORD, D. C. 1971 Analysis of scallop patterns by simulation under controlled conditions. *J. Geol.* **79**, 52.

HUGHMARK, G. A. 1972 Turbulent heat and mass transfer from rough surfaces. *A.I.Ch.E. J.* **18**, 667.

KENNEDY, J. F. 1964 The formation of sediment ripples in closed rectangular channels and in the desert. *J. Geophys. Res.* **69**, 1517.

MOTZFELD, H. 1937 Die turbulente Strömung an wellingen Wänden. *Z. angew. Math. Mech.* **17**, 193.

NEWMAN, B. G. 1961 The deflection of plane jets by adjacent surfaces – Coanda effect. *Boundary Layer and Flow Control* (ed. G. V. Lachmann), pp. 232–264. Pergamon.

RUDNICKI, J. 1960 Experimental work on flute development. *Speleologia (Warsaw)*, **2**, 17.

SAWYER, R. A. 1962 The flow due to a two-dimensional jet issuing parallel to a flat plate. *J. Fluid Mech.* **9**, 543.

SCHLICHTING, H. 1937 Experimental investigation of the problem of surface roughness. *N.A.C.A. Tech. Memo.* no. 823. (See also 1936 *Ing. Arch* **7**, 1.)

SCHLICHTING, H. 1968 *Boundary Layer Theory*, pp. 578–583. McGraw-Hill.

SEIFERTH, R. & KRUGER, W. 1950 Überraschend höhe Reibungsziffer einer Fernwasserleitung. *VDI Z.* **92**, 189.

WEIDERHOLD, W. 1949 Über den Einfluss von Rohrablagerungen auf den hydraulischen Druckabfall. *Gas-u. Wasserfach.* **90**, 634.

(*a*)

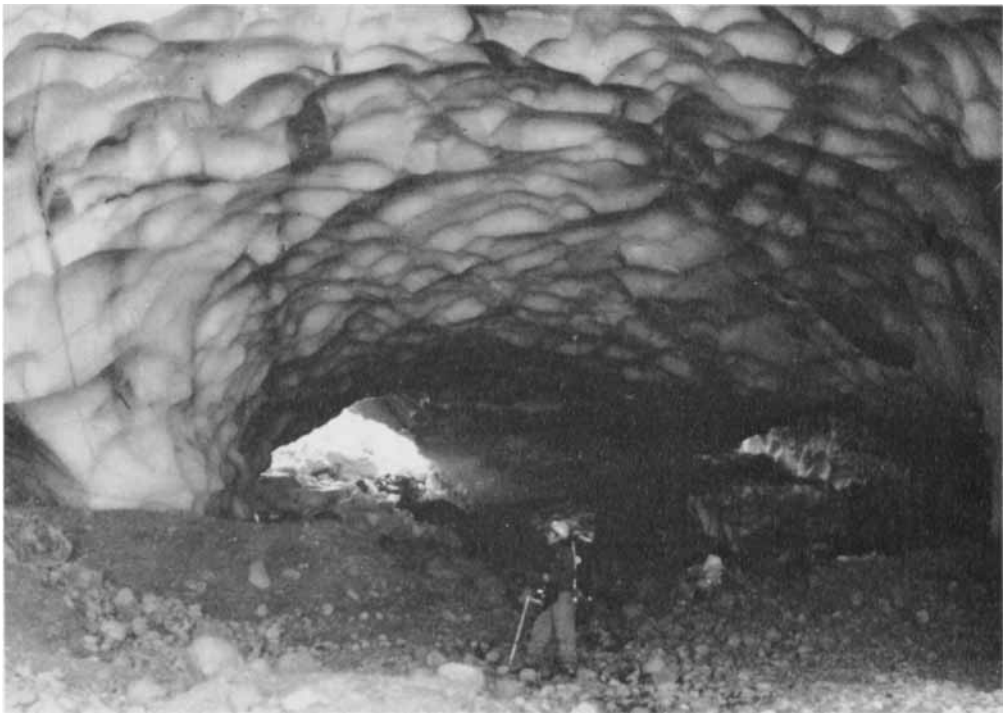

(*b*)

FIGURE 1. (*a*) Naturally occurring scallops and flutes on limestone. Pollnagullum Cave, Ireland. Reproduced with permission of the University of Bristol Speleological Society. Photography by D. M. M. Thomson. (*b*) Naturally occurring scallops in ice. Paradise Ice Caves, Washington. Photo by C. H. Anderson, Jr.

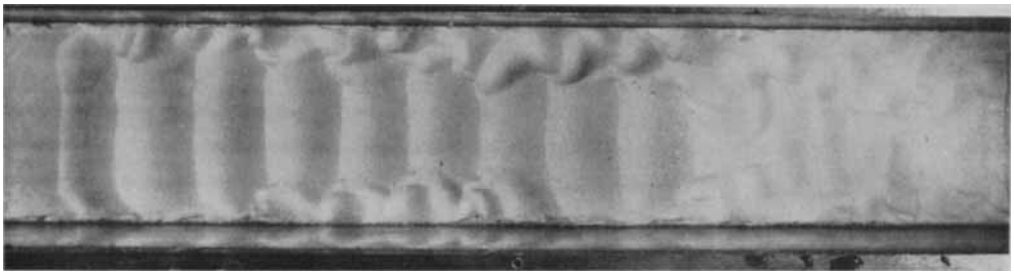

FIGURE 3. Experiment 2 with 'stable' 2 in. flutes after $0{\cdot}8L$ dissolution. The 1 in. pattern has been destroyed. Side-wall effects have become pronounced but the 2 in. flutes retain their character in the centre of the channel. (The longitudinal stripes in figures 3 and 4 are due to ripples on the water surface through which the photograph was taken with the flow stopped.)

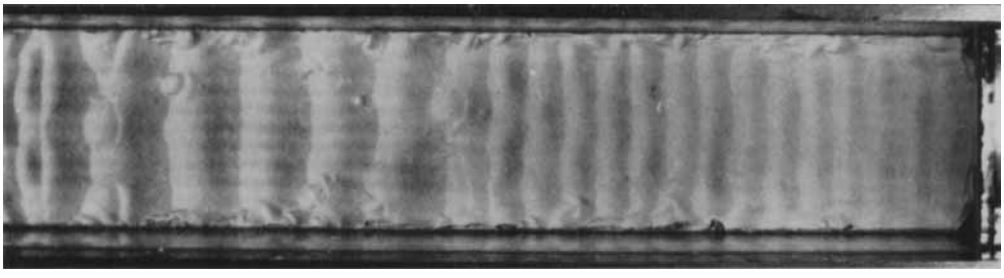

FIGURE 4. Experiment 3 with 'stable' 1 in. flutes after $1{\cdot}4L$ dissolution. The 2 in. pattern is being destroyed by the generation of new small-scale features.

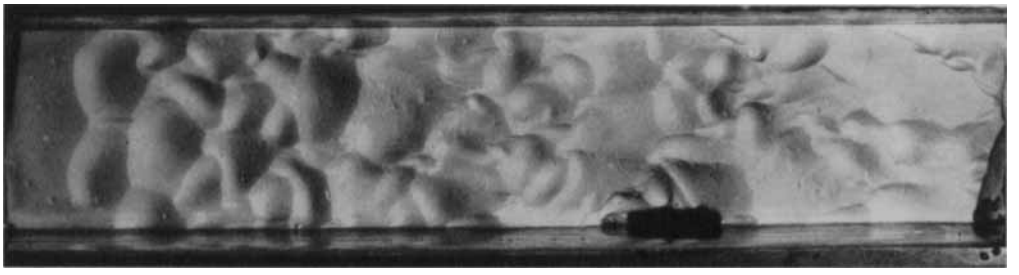

(*a*)

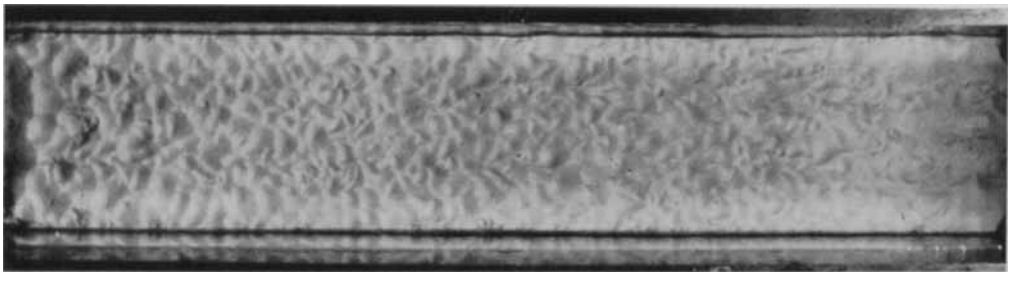

(*b*)

FIGURE 5. Experiments 1 and 4 after scallop patterns have developed. (*a*) Experiment 1 at 45 cm/s and 15·7 °C. (*b*) Experiment 4 at 116 cm/s and 32·5 °C.

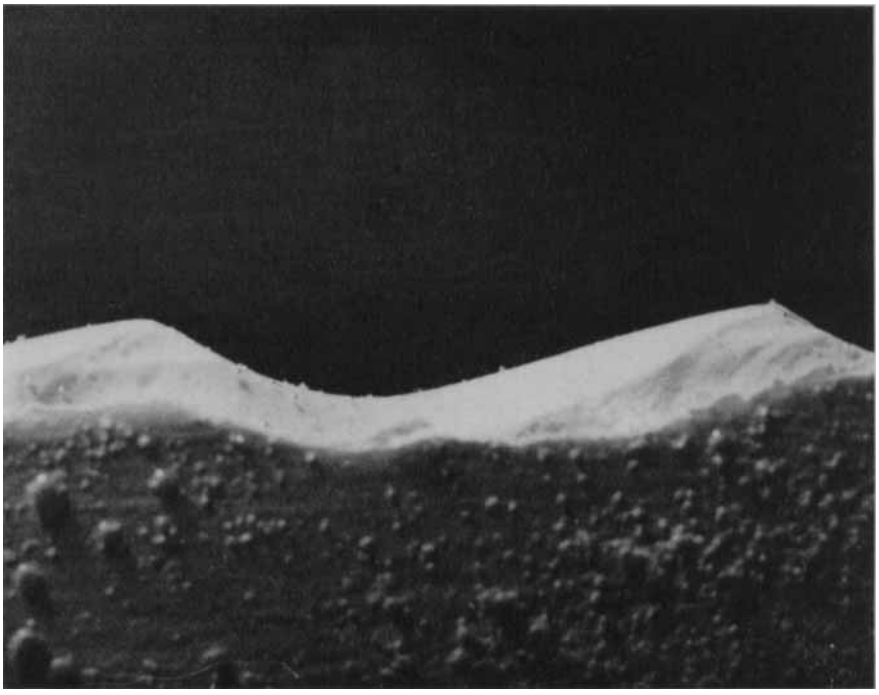

FIGURE 7. Typical flute profile, photographed *in situ*.